

Journal of Biomedical Optics

SPIDigitalLibrary.org/jbo

Tri-modal confocal mosaics detect residual invasive squamous cell carcinoma in Mohs surgical excisions

Dan Gareau
Anna Bar
Nicholas Snaveley
Ken Lee
Nathaniel Chen
Neil Swanson
Eric Simpson
Steve Jacques

Tri-modal confocal mosaics detect residual invasive squamous cell carcinoma in Mohs surgical excisions

Dan Gareau,^{a,b} Anna Bar,^a Nicholas Snavely,^a Ken Lee,^a Nathaniel Chen,^b Neil Swanson,^a Eric Simpson,^a and Steve Jacques^{a,b}

^aOregon Health & Science University, Department of Dermatology, CH16D, 3303 SW Bond Avenue, Portland, Oregon 97239

^bOregon Health & Science University, Department of Biomedical Engineering, CH16D, 3303 SW Bond Avenue, Portland, Oregon 97239

Abstract. For rapid, intra-operative pathological margin assessment to guide staged cancer excisions, multimodal confocal mosaic scan image wide surgical margins (approximately 1 cm) with sub-cellular resolution and mimic the appearance of conventional hematoxylin and eosin histopathology (H&E). The goal of this work is to combine three confocal imaging modes: acridine orange fluorescence (AO) for labeling nuclei, eosin fluorescence (Eo) for labeling cytoplasm, and endogenous reflectance (R) for marking collagen and keratin. Absorption contrast is achieved by alternating the excitation wavelength: 488 nm (AO fluorescence) and 532 nm (Eo fluorescence). Superposition and false-coloring of these modes mimics H&E, enabling detection of cutaneous squamous cell carcinomas (SCC). The sum of mosaic Eo + R is false-colored pink to mimic the appearance of eosin, while the AO mosaic is false-colored purple to mimic the appearance of hematoxylin in H&E. In this study, mosaics of 10 Mohs surgical excisions containing invasive SCC, and five containing only normal tissue were subdivided for digital presentation equivalent to 4× histology. Of the total 50 SCC and 25 normal sub-mosaics presented, two reviewers made two and three type-2 errors (false positives), respectively. Limitations to precisely mimic H&E included occasional elastin staining by AO. These results suggest that confocal mosaics may effectively guide staged SCC excisions in skin and other tissues. © 2012 Society of Photo-Optical Instrumentation Engineers (SPIE). [DOI: 10.1117/1.JBO.17.6.066018]

Keywords: cancer screening; confocal; fluorescence; imaging; Mohs surgery; squamous cell carcinoma.

Paper 12042 received Jan. 18, 2012; revised manuscript received Apr. 27, 2012; accepted for publication May 1, 2012; published online Jun. 6, 2012.

1 Introduction

New modalities for rapid noninvasive optical imaging of skin cancers include Raman spectroscopy,^{1,2} fluorescence polarization,³ multiphoton,^{4,5} fluorescence lifetime,⁶ fluorescence imaging,^{7,8} optical coherence tomography,⁹ and reflectance confocal microscopy.¹⁰ Confocal microscopy is the most clinically practical technology, with high resolution and sectioning comparable with that of conventional histology. Nuclear, cellular and structural detail is noninvasively imaged in thin optical sections (1 to 5 μm) with high lateral resolution (0.5 to 1 μm) by objective lenses with high numerical apertures of 0.7 to 1.4 and magnifications of 20 to 100×. Recent studies demonstrate excellent correlation between confocal images and histopathology for normal skin and malignant lesions in freshly excised tissue.¹¹

Mohs surgery of the skin, a well-developed staged procedure where the surgeon also serves as the pathologist, represents an ideal testing ground for rapid diagnostics. Micrographic tumor removal achieves minimal damage to the surrounding normal tissue by a series of residual tumor excisions guided by frozen histopathology. Rapid micrographic pathology represents an opportunity for confocal microscopy of whole tissue excisions. By stitching square raster-scanned fields of view together, a 12 × 12 mm mosaic can be produced in 9 min,¹² which is similar to a 2× histological view of a Mohs excision. A recently developed “strip mosaicing” technique is even faster, producing a 10 × 10 mm mosaic in about 3 min.¹³ In strip mosaicing, the

slow-axis scanning galvanometer is fixed on the optical axis while the fast polygon scans a stationary line in the tissue. The sample is physically scanned perpendicular to the stationary line in the focal plane to acquire long rectangular images are stitched together in less time than square images.¹³ The long rectangular images conveniently have no field curvature in their long (mechanically scanned) axis. These are rapid techniques compared to histology, which takes 20 to 45 min.¹² Adapting the technique to guide excision of different cancer types would save more tissue and possibly enable new surgeries. Expanding within the framework of Mohs surgery, the pathologic profile of squamous cell carcinoma may be applicable beyond the skin.

The overall cure rate of Mohs surgery in skin is 96.6%¹⁴ and the high diagnostic accuracy depends heavily on imaging. For the two main non-melanoma skin cancers treated with Mohs surgery [basal cell carcinoma (BCC) and squamous cell carcinoma (SCC)], precise intra-operative micrographic “staging” minimizes disfiguring side effects. Confocal mosaics can locate the smallest infiltrative single-cell strands of BCC,¹¹ but SCC is more difficult, mirroring the trend in histopathology-guided treatment -the more easily detected cancer (BCC) is treated with a 99.1% cure rate,¹⁴ while SCC has a 94.8% cure rate.¹⁴ BCC tumors are circumscribed, densely nucleated, discreet bodies, where SCC tumor is a dysplasia grade continuum down-grade from sun damage-related actinic keratosis. SCC lacks the high nuclear-to-cytoplasmic ratio typical of BCC, and is therefore not well-detected with a single fluorescent nuclear stain. Hence, SCC is a more complicated diagnosis than

Address all correspondence to: Dan Gareau, Oregon Health & Science University, Department of Dermatology, CH16D, 3303 SW Bond Avenue, Portland, Oregon 97239. Tel: +1 503 708 7078; Fax: +1 212 308 0854; E-mail: dan@dangareau.net.

BCC, requiring additional pathometric evaluation of cytoplasm which has not been achieved by previous work using only the nuclear stain.¹¹ Cell size (including cytoplasm), nuclear-to-cytoplasmic ratio, and the state of differentiation are characteristics evaluated in populations of cells for SCC diagnosis. SCC cells have an atypical size distribution (pleomorphism) and/or an atypical nuclear-to-cytoplasmic ratio. Conventional histopathological evaluation of these traits uses a diagnostic application of two separate stains for nuclei (hematoxylin) and for everything else (eosin) including cytoplasm and structural components such as collagen and keratin. Eosin staining is particularly important for evaluating the cellular pathology of invasive SCC. We present an important step in a series of advances in confocal mosaic microscopy as an augmentation or alternative to frozen histology the use of eosin (Eo) in fluorescence mode to identify cytoplasm in confocal mosaics. Thus far, only two contrast mechanisms have been investigated for (1) nuclei in fluorescence mode with acridine orange¹² (AO), and (2) collagen and keratin in endogenous reflectance (R) mode.¹⁵ The combination of these two modes works to detect BCC because the nuclear stain provides a clear positive indicator of the dense nuclear morphology on the background of counter contrasted collagen and keratin. A third stain is needed for SCC detection because reflectance fails to label cytoplasm strongly enough. Though reflectance has been reported to label cytoplasm, the magnitude of reflectance from collagen is approximately 4× larger. This number was extracted from the pixel values from epidermis (for cytoplasm) and dermis (for collagen) in Ref. 15 [Fig. 1(a)]. Therefore, an image that attempts to show both collagen and cytoplasm would either show the collagen as saturated (if adjusted for a reasonable contrast of cytoplasm) or show the cytoplasm as too dark (if adjusted for a reasonable contrast of collagen). In this paper, the need for increased cytoplasmic contrast is addressed by implementing fluorescence staining with Eo in whole-tissue in combination with the previously described AO¹² and reflectance¹⁵ contrast. Tri-modal confocal microscopy provides better SCC pathology than single or dual-mode techniques in skin excisions by revealing cytoplasmic detail in addition to nuclear (AO) and structural (R) details. The tar-

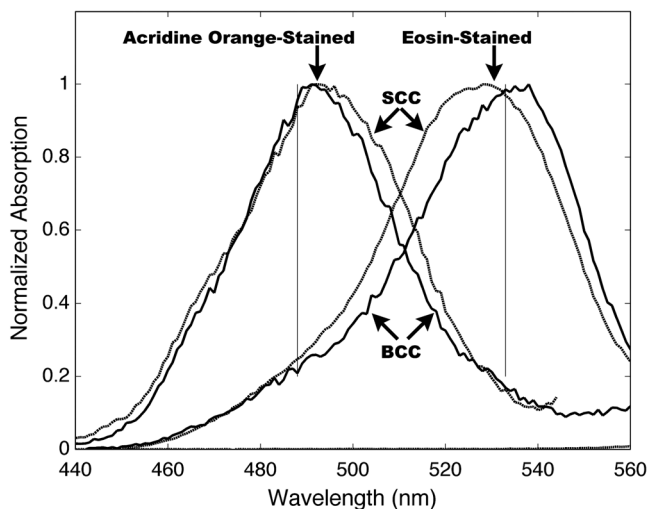


Fig. 1 The absorption spectra of squamous cell carcinoma (SCC) and basal cell carcinoma (BCC) tissue stained with either acridine orange or eosin. Unstained tissue was also measured as a control, but the normalized absorption is too small to be visible on this graph.

geted cellular pathology for invasive SCC consists of abnormal nests of cancer cells in the dermis. To visualize them, we present the following method.

2 Materials and Methods

Samples from a total of 17 patients were obtained with informed consent under the OHSU IRB-approved protocol. Inclusion criteria consisted of the presence of invasive SCC, as verified by the intra-operative histopathology produced during the Mohs procedure. Since each patient had a positive stage (containing SCC) at the beginning of the surgery, and a negative stage (containing only normal tissue) at the end of the surgery the normal confocal mosaics were derived from the same patient population. Since the histology was viewed by co-author Dan Gareau prior to confocal imaging, the confocal imaging was not “blind,” to the gold standard. During the entire process of development and clinical testing, we imaged three rounds of samples: the first round consisting of one BCC tumor and one SCC tumor, the second round consisting of five SCC samples to fine-tune the prototype microscope, and the third round consisting of 10 SCC samples and five normal samples which were evaluated by clinical co-investigators Anna Bar and Nicholas Snaveley.

In the first round, a single BCC tumor and SCC tumor were each bisected and impaled on four pins. Each tissue sample was nearly pure tumor (from a de-bulking procedure), and approximately 5 mm in size. The samples were immersed in AO or stock Eo solution (1 mM aqueous, pH 6.0) for 1 min., and then placed in a spectrophotometer (Fluorolog-3, S. A. Instruments Inc., Edison, NJ). Emission (>570 nm) was measured while the internal scanning slit monochromator varied the excitation wavelength over the spectral range in Fig. 1. The measured fluorescence intensity (which was directly proportional to the absorption coefficient) was normalized for each sample, and is shown in (Fig. 1). After the preliminary spectroscopy work dictated the optical design choices of laser wavelengths and stains, we developed a tri-modal confocal microscope and staining procedure to image three critical tissue components independently. Table 1 summarizes the approach.

The tissue staining procedure consisted of the following five steps:

1. 30-s rinse in 95% ethanol for dehydration
2. 30-s soak in stock Eo solution (identical to that used in the gold standard histopathology)
3. 30-s rinse in isotonic phosphate-buffered saline solution
4. 30-s soak in AO solution (1 mM, in phosphate buffered saline at pH 6.0 controlled by addition of HCl), and

Table 1 Optical contrast scheme for tri-modal confocal microscopy.

Tissue component	Confocal mode	λ Illumination	Stain
Cytoplasm	Fluorescence	532 nm	Eosin
Nuclei	Fluorescence	488 nm	Acridine Orange
Collagen/Keratin	Reflectance	488 nm	(no stain)

5. 5-s rinse in isotonic phosphate-buffered saline solution.

After staining, the samples were fixed on the mechanical stage (similarly to our previously described protocol¹²) and imaged by the prototype confocal microscope.

We adapted a commercially available *ex-vivo* confocal imager to complete this study. The hardware was composed of a breadboard version of the VivaScope 2500 (Lucid, Rochester NY) which was augmented with a 30-mW, 488-nm diode laser (CLAS0488-025PP00, Blue Sky Research, Milpitas, CA) and a 50-mW, 532-nm diode laser (GMLN-532-50AC,

Lasermate Group Inc., Pomona, CA) that were joined in the same path with a dichroic filter (LM01-503-25, Semrock Inc., Rochester, NY). A dual narrow band-pass dichroic filter (Di01-T488/532-13-15-0.5, Semrock Inc., Rochester, NY) transmitted the excitation wavelengths toward the sample, and reflected the emission wavelengths toward the fluorescence detector (R7400U-20, Hammamatsu Inc.). The detector was shielded from stray excitation light contamination by blocking filters for 532-nm and 488-nm operation (BLP01-532-5-10 and BLP01-488-5-10, respectively, Semrock Inc., Rochester, NY), and shielded from out-of-focus light by a confocal pinhole aperture. Previously reported techniques¹⁵ were implemented for the

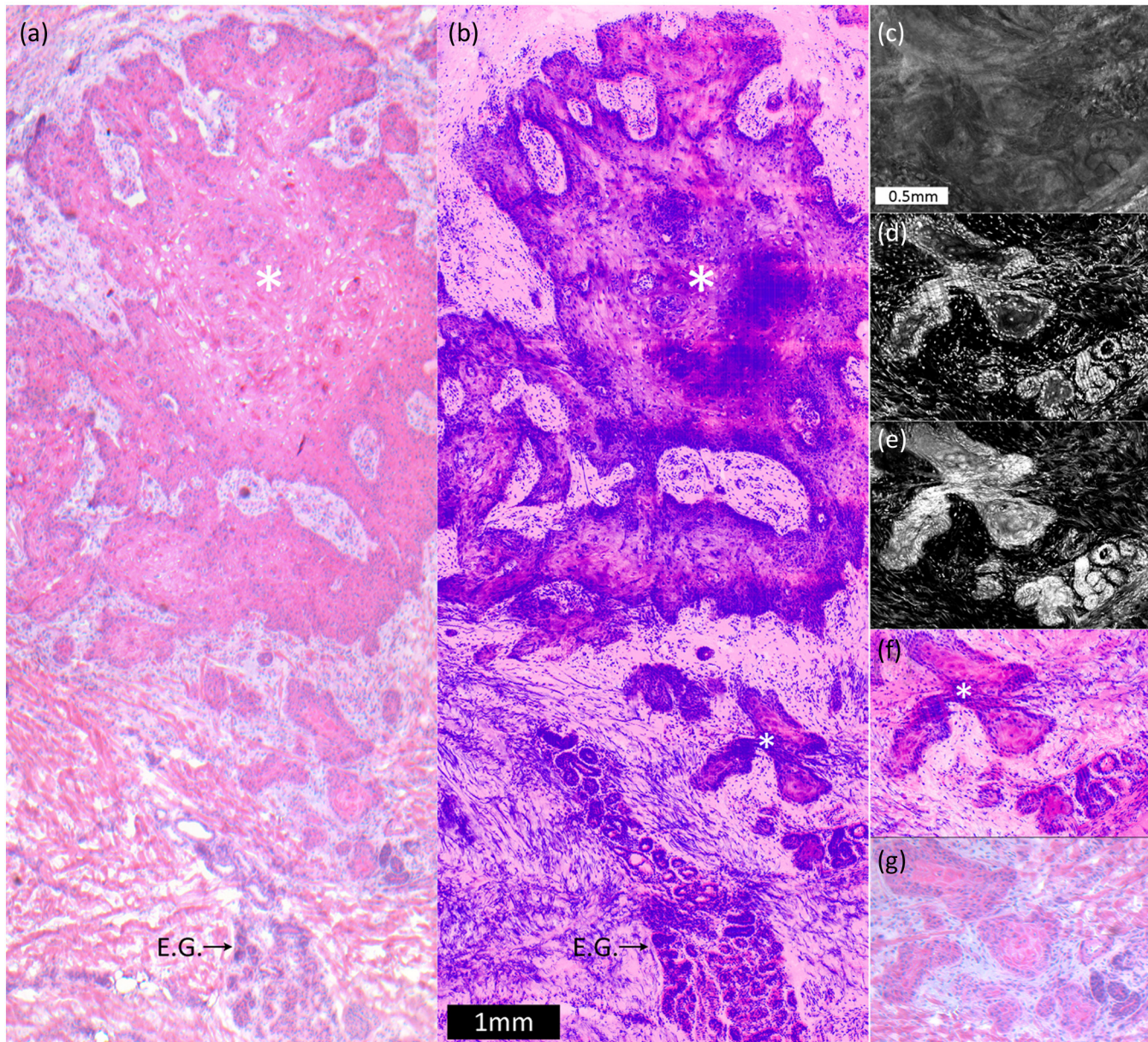


Fig. 2 Invasive squamous cell carcinoma in the dermis. Histopathology with an approximately 4x field of view; (a) shows a large invasive tumor focus marked by the asterisk (*) as well as an eccrine gland in the dermis (E.G.). In the lower left of the image, collagen and elastin fibrous material can be seen. The 4x histology had resolution of about $5\ \mu\text{m}$ resolution when displayed on a typical computer screen. The corresponding confocal sub-mosaic (b) shows excellent correlation. An additional smaller tumor is marked by a smaller asterisk (*). The smaller tumor is digitally magnified (and slightly rotated for display) in reflectance mode to show structure (c), in acridine orange fluorescence mode to show nuclei (d) and eosin fluorescence-mode to show cell bodies (e). The composite image (f) correlates with optically zoomed histopathology (g) and shows cellular resolution at 30x, which is the key pathological feature.

reflectance channel optics, the step-and-capture routine that acquired the mosaic tiles, fixing the whole-mount tissue specimen on the stage and for stitching the mosaic tiles in software.

Digital staining (the combination of the imaging modes in a false-colored image) was implemented in a manner similar to one previously reported¹⁵ that was adapted to accommodate three modes. In Eq. (1), the digitally stained confocal mosaic (DSCM) is a function of x - y position and bit depth k where the colors of pink (to mimic eosin) and purple (to mimic hematoxylin) are: $E = [1, 0.55, 0.88]$ and $H = [0.30, 0.20, 1]$, respectively [red ($k = 1$), green ($k = 2$), blue ($k = 3$), respectively], where $F1$ and $F2$ were the single mode confocal mosaics of AO fluorescence and Eo fluorescence, respectively, and R was the reflectance mosaic.

$$DSCM_{x,y,k} = 1 - F1_{x,y}(1 - H_k) - (F2_{x,y} + R_{x,y})(1 - E_k). \quad (1)$$

A total of 13 SCC samples and seven normal samples were imaged and a single tri-modal mosaic was produced for each sample. Three SCC mosaics and three normal mosaics were excluded due to tissue tearing during mechanical fixation to the confocal microscope, which compromised the ability to correlate these confocal mosaics to the corresponding histopathology. This yielded a test set of 10 SCC and five normal samples.

3 Clinical Review

Clinical review was conducted as previously described.¹¹ Briefly, our two Mohs surgeons (co-authors Bar and Snavely) reviewed randomly ordered confocal mosaics, marking each as SCC or normal. The sub-mosaics were reviewed and for each sub-mosaic, each of the two reviewers (separately) marked a positive (containing tumor) or negative (containing only normal tissue) diagnostic screening result. This review of the confocal sub-mosaics was completed at least three weeks after the reviewers had last seen the correlating histopathology (i.e., three weeks after the surgical procedure), so there was likely no recollection of the case to interfere with the “blinded” nature of the confocal review. Co-author Dan Gareau correlated the randomly ordered answers with the results of the histology originally produced during Mohs surgery and scored each mark a true positive, false positive, true negative, or false negative. The sensitivity and specificity of the data set were calculated using standard methods.¹⁶

4 Preliminary Results

The rationale for the approach in Table 1 stemmed from preliminary spectroscopy results which showed absorption contrast differentially excite fluorescence from nuclei and cytoplasm. We measured fluorescence emission profiles (not shown) that were similar between the two stains, so we chose absorption contrast. Figure 1 shows the absorption spectra for our two stains in tissue. As a control, an unstained piece of BCC tumor, normalized by the same factor used in the BCC with AO staining, showed negligible absorption.

5 Results

The confocal mosaics appeared similar to 2× H&E histology, except they occasionally had artifact grid lines from the mosaic construction and AO staining of elastin in the dermis. In the study set, 10 samples containing invasive SCC and five samples

Table 2 Clinical review result.

Confocal screening result		↓	↓	
Reviewer #1, Bar				
Histology screening result	→	Positive	2	25
	→	Negative	48	0
Reviewer #2, Snavely				
Histology screening result	→	Positive	3	25
	→	Negative	47	0

containing normal tissue were imaged. From the mosaics, 50 sub-mosaics containing invasive SCC and 25 containing only normal dermis, with cellular structures such as eccrine glands, sebaceous glands and hair follicles were prepared. Sub-mosaics consisted of cropped regions of the full mosaics which had a field of view of about 5 mm. This size was chosen to mimic 4× histopathology because our previous report¹¹ concluded that for BCC, this magnification yielded high sensitivity/specificity for tumor detection. Figure 2 shows a sample sub-mosaic of invasive SCC, as well as a zoomed in view of the individual modes and their addition.

Table 2 shows the results of the clinical review. The two reviewers (Bar and Snavely) evaluated all the confocal sub-mosaics correctly except for two and three false positives, respectively. The calculated diagnostic value from Table 1 is 100% for sensitivity, and 96% and 94% for specificity for Bar and Snavely, respectively.

6 Discussion

Tri-modal confocal mosaics mimic histopathology in appearance, and may be of similar diagnostic value. We found in this study that AO and Eo provide confocal contrast in whole tissue similar to hematoxylin and eosin in conventional histology except for the following limitations: (1) We were not able to achieve eosin staining the dermis in whole tissue like it does in histology with our staining protocol. (2) AO occasionally [as in Fig. 2(b) in the lower left] labeled elastin fibers in the dermis. This was unexpected and does not mimic the contrast of hematoxylin in histology. AO is known to label nuclei by selectively intercalating between nuclear protein side-chains, but the mechanism by which AO labels elastin in this work is unknown. Current and future studies aim to determine if this is consistent and/or avoidable. The labeling of elastin by AO may be a function of the time and concentration of immersion when staining, but is definitely a weakness in the clinical translation of this technique because it represents a difference from what surgeons/pathologists are accustomed to seeing.

The small number of trials in this study and the selection of only normal versus invasive SCC (i.e., exclusion of more subtle *in situ* disease) are by no means a comprehensive evaluation. A larger multicenter clinical trial is needed to fully evaluate this technique. However, the 95% confidence interval for the average sensitivity from the 75 sub-mosaics evaluated is 0.86-to-1 as calculated by the

Clopper and Pearson method.¹⁶ This means there is a low probability (<5%) that the sensitivity is unacceptable (worse than 0.86) according to the clinical requirements. Further studies are needed to determine if the technique is accurate as comparable to the overall cure rate for Mohs surgery, which is 0.97.¹⁴

Compared to histology, the confocal tri-modal approach is rapid and cheap, but tri-modal confocal mosaics also produce less tissue-processing artifact. For instance, Fig. 2(a) shows large void areas in the H&E that are not present in the confocal mosaic. These void areas are artifacts of frozen tissue processing and their absence in the confocal mosaic speaks to the attractive nature of confocal imaging on tissue in a more natural and less processed whole-state. We expect this technique to be applicable to cancer excisions beyond the skin such as in excisions of oral mucosal lesions, thyroid nodules, parathyroid glands, and bone during head-and-neck surgery, needle core-biopsies and lumpectomies of breast, and intra-operative biopsies of liver, kidney and bladder that have been imaged with confocal microscopy.¹⁷⁻¹⁹

Acknowledgments

Co-author Dan Gareau was supported during this work by NIH 5-T32-CA106195.

References

1. A. Nijssen et al., "Discriminating basal cell carcinoma from perilesional skin using high wave-number Raman spectroscopy," *J. Biomed. Opt.* **12**(3), 034004 (2007).
2. C. A. Lieber et al., "Raman microscopy for skin cancer detection," *J. Biomed. Opt.* **13**, 024013 (2008).
3. A. N. Yaroslavsky et al., "Fluorescence polarization of tetracycline derivatives as a technique for mapping nonmelanoma skin cancers," *J. Biomed. Opt.* **12**(1), 014005 (2007).
4. J. Paoli et al., "Multiphoton laser scanning microscopy on non-melanoma skin cancer: morphologic features for future non-invasive diagnostics," *J. Invest. Dermatol.* **128**(5), 1248-1255 (2007).
5. S. J. Lin et al., "Discrimination of basal cell carcinoma from normal dermal stroma by quantitative multiphoton imaging," *Opt. Lett.* **31**(18), 2756-2758 (2006).
6. N. P. Galletly et al., "Fluorescence lifetime imaging distinguished basal cell carcinoma from surrounding uninvolved skin," *Br. J. Dermatol.* **159**(1), 152-161 (2008).
7. M. B. Ericson et al., "Bispectral fluorescence imaging combined texture analysis and linear discrimination correlation with histopathologic extent of basal cell carcinoma," *J. Biomed. Opt.* **10**(3), 034009 (2005).
8. B. Stenquist et al., "Bispectral fluorescence imaging of aggressive basal cell carcinoma combined with histopathological mapping: a preliminary study indicating a possible adjunct to Mohs micrographic surgery," *Br. J. Dermatol.* **154**(2), 305-309 (2006).
9. J. M. Olmedo et al., "Optical coherence tomography for the characterization of basal cell carcinoma in vivo: a pilot study," *J. Am. Acad. Dermatol.* **55**(3), 408-412 (2006).
10. S. Gonzalez, M. Gill, and A. C. Halpern, Eds., *Reflectance Confocal Microscopy of Cutaneous Tumors*, Informa U.K. Ltd., London (2008).
11. D. S. Gareau et al., "Sensitivity and specificity for detecting basal cell carcinomas in Mohs excisions with confocal fluorescence mosaicing microscopy," *J. Biomed. Opt.* **14**(3), 1-7 (2009).
12. D. S. Gareau et al., "Confocal mosaicing microscopy in Mohs skin excisions: feasibility of rapid surgical pathology," *J. Biomed. Opt.* **13**(5), 054001 (2008).
13. S. Abeytunge et al., "Rapid confocal imaging of large areas of excised tissue with strip mosaicing," *J. Biomed. Opt.* **16**(5), 050504 (2011); .
14. F. E. Mohs, *Chemosurgery: Microscopically Controlled Surgery For Skin Cancer*, p. 55, Thomas, Springfield, Ill (1978). 978-0-398-03725-3
15. D. S. Gareau, "The feasibility of digitally stained multimodal confocal mosaics to simulate histopathology," *J. Biomed. Opt.* **14**(3), 034050 (2009).
16. C. Clopper and E. S. Pearson, "The use of confidence or fiducial limits illustrated in the case of the binomial," *Biometrika* **26**, 404-413 (1934)
17. M. T. Tilli et al., "Real-time imaging and characterization of human breast tissue by reflectance confocal microscopy," *J. Biomed. Opt.* **12**(5), 051901 (2007).
18. W. M. White et al., "A novel noninvasive imaging technique for intraoperative assessment of parathyroid glands: confocal reflectance microscopy," *Surgery* **128**(6), 1088-1100 (2000).
19. H. Makhlof et al., "Multispectral confocal microendoscope for in vivo and in situ imaging," *J. Biomed. Opt.* **13**(4), 044016 (2008).